



ARTICLE

Scutellarin suppresses triple-negative breast cancer metastasis by inhibiting TNF α -induced vascular endothelial barrier breakdown

Xi-yu Mei¹, Jing-nan Zhang¹, Wang-ya Jia¹, Bin Lu¹, Meng-na Wang¹, Tian-yu Zhang¹ and Li-li Ji¹

Triple-negative breast cancer (TNBC) is an aggressive subtype of breast cancer with high vascularity and frequent metastasis. Tumor-associated abnormal vasculature was reported to accelerate TNBC metastasis. Scutellarin (SC) is a natural flavonoid with a cardiovascular protective function. In this study, SC reduced TNBC metastasis and alleviated tumor-associated vascular endothelial barrier injury in vivo. SC rescued the tumor necrosis factor- α (TNF α)-induced diminishment of endothelial junctional proteins and dysfunction of the endothelial barrier in vitro. SC reduced the increased transendothelial migration of TNBC cells through a monolayer composed of TNF α -stimulated human mammary microvascular endothelial cells (HMMECs) or human umbilical vein endothelial cells (HUVECs). TNF α induced the nuclear translocation of enhancer of zeste homolog-2 (EZH2), and its chemical inhibitor GSK126 blocked TNF α -induced endothelial barrier disruption and subsequent TNBC transendothelial migration. TNF receptor 2 (TNFR2) is the main receptor by which TNF α regulates endothelial barrier breakdown. Extracellular signal-regulated protein kinase (ERK)1/2 was found to be downstream of TNF α /TNFR2 and upstream of EZH2. Additionally, SC abrogated the TNFR2-ERK1/2-EZH2 signaling axis both in vivo and in vitro. Our results suggest that SC reduced TNBC metastasis by suppressing TNF α -initiated vascular endothelial barrier breakdown through rescuing the reduced expression of junctional proteins by regulating the TNFR2-ERK1/2-EZH2 signaling pathway.

Keywords: TNBC; metastasis; endothelial barrier breakdown; TNF α ; scutellarin

Acta Pharmacologica Sinica (2022) 43:2666–2677; <https://doi.org/10.1038/s41401-022-00873-y>

INTRODUCTION

Triple-negative breast cancer (TNBC) is an aggressive breast cancer defined by the lack of hormone receptors and human epidermal growth factor receptor 2 (HER2) [1]. One in eight to ten women will develop breast cancer during their lifetime, while ~15% of patients suffer from TNBC [1, 2]. Most importantly, the incidence of breast cancer metastasis in TNBC patients is obviously higher than that in other breast cancer subtypes [3]. The median overall survival in metastatic TNBC is ~1 year, but it is ~5 years in the other 2 subtypes (hormone receptor-positive/HER2-negative, HER2-positive) [2]. Due to the absence of well-defined molecular targets, the standard treatment of TNBC is limited to surgery, generic adjuvant cytotoxic chemotherapy and radiotherapy, but TNBC is still incurable with these currently available therapies [4]. Therefore, unraveling the underlying mechanism of TNBC metastasis is of great clinical significance for its subsequent therapeutic intervention.

Metastasis is a complex process that develops as a result of the interaction between tumor cells and the surrounding microenvironment, which consists of tumor cells, immunocytes, cancer-associated vessels, fibroblasts and various cytokines [5]. In this tumor microenvironment, persistent inflammation and aberrant

vasculature are reported to be two typical features discovered in some previous studies [6].

Vessels supply oxygen and nutrients for solid tumors. Thus, anti-angiogenesis has been proposed to be a well-known therapeutic strategy for cancer treatment in recent decades [7]. However, this kind of therapy has not achieved complete success in past clinical practice, and sometimes it even accelerated the progression of tumors in refractory breast cancer [7, 8]. In normal vasculature, the inner wall is composed of a confluent endothelial cell (EC) monolayer with integral intercellular junctions. Tight junctions (TJs), including the claudin family, and adherens junctions (AJs), mainly organized by vascular endothelial cadherin (VE-cadherin), are two major types of junctional complexes in the endothelium [9]. In contrast, the tumor vasculature is disorganized, immature and permeable, with disrupted junctions and uncontrolled vascular homeostasis [10]. Because of hypoxia and low perfusion, abnormal tumor vasculature promotes tumor metastasis and reduces the diffusion of drugs [11]. A previous study has shown that the normalization of tumor vessels may be favorable for the amelioration of the tumor microenvironment in solid tumors [12]. In particular, the mammary gland vasculature has abundant capillaries, and it is always remodeled according to changes in the

¹The MOE Key Laboratory for Standardization of Chinese Medicines, Shanghai Key Laboratory of Compound Chinese Medicines and The SATCM Key Laboratory for New Resources and Quality Evaluation of Chinese Medicines, Institute of Chinese Materia Medica, Shanghai University of Traditional Chinese Medicine, Shanghai 201203, China
Correspondence: Li-li Ji (lichenyue1307@126.com)

These authors contributed equally: Xi-yu Mei, Jing-nan Zhang.

Received: 29 June 2021 Accepted: 18 January 2022

Published online: 28 February 2022

hormonal environment [13]. Thus, it is essential to investigate the potential effect of the abnormal vasculature on TNBC metastasis.

Tumor necrosis factor- α (TNF α) is always highly expressed in biopsies and plasma of patients with multiple advanced cancers, including TNBC, and it contributes to the recruitment of immune cells such as myeloid-derived suppressor cells, tumor-associated macrophages and immature dendritic cells [14, 15]. Anti-TNF α antibodies, including infliximab and etanercept, are reported to inhibit murine pancreatic cancer metastasis *in vivo* [16]. TNF α production was reported to be associated with poor prognosis and cachexia/asthenia in patients with various tumors [17]. Moreover, clinical trials have shown that the TNF α inhibitor etanercept may be a potential therapeutic drug for metastatic breast cancer [18]. Recent studies suggest that TNF α promotes the survival and proliferation of malignant cells either directly by activating the NF- κ B signaling pathway in cancer cells or indirectly by inducing immunosuppression and matrix degradation [19, 20]. However, whether TNF α accelerates TNBC metastasis by destroying the integrity of the microvascular barrier in tumors is still not clear.

Natural flavonoid scutellarin (SC) is the only compound in the listed drug breviscapine (including tablet and injection) indexed in the China Pharmacopoeia [21]. SC has an excellent ability to protect the vascular system, and it is commonly used for treating angina pectoris, pulmonary heart disease, chronic heart failure, coronary heart disease and myocardial infarction [22]. Previous studies showed that SC suppressed the proliferation and metastasis of some types of tumors, including colorectal cancer, liver cancer and bladder cancer [23–25]. There is still no report about the inhibitory effect of SC on TNBC growth or metastasis. In this study, the inhibitory effect of SC on TNBC metastasis mediated by suppressing TNF α -initiated vascular endothelial barrier breakdown and the associated mechanism were investigated.

MATERIALS AND METHODS

Antibodies and chemical reagents

Antibodies against VE-cadherin, α -smooth muscle actin (α -SMA), enhancer of zeste homolog-2 (EZH2), extracellular signal-regulated protein kinase (ERK)1/2, phospho-ERK1/2 (Thr202/Tyr204), p38 and phospho-p38 (Thr180/Tyr182) were purchased from Cell Signaling Technology (Danvers, MA). Antibodies against Lamin B1 were purchased from Abways (Shanghai, China). Antibodies against β -actin were purchased from HuaBio (Hangzhou, China). Antibodies against claudin-1, occludin, platelet/endothelial cell adhesion molecule-1 (PECAM-1/CD31), TNF α and TNF receptor 2 (TNFR2) were purchased from Santa Cruz (Santa Cruz, CA). TNF α was obtained from PeproTech Inc. (Rocky Hill, NJ). Peroxidase-conjugated goat anti-rabbit immunoglobulin G (IgG) (H + L) and anti-mouse IgG (H + L) were purchased from Jackson ImmunoResearch (West Grove, PA). Alexa Fluor 647 phalloidin- or Alexa 488-labeled goat anti-rabbit antibody, Alexa 488-labeled goat anti-mouse antibody or Alexa 568-labeled goat anti-rabbit antibody were purchased from Life Technology (Carlsbad, CA). NE-PER nuclear and cytoplasmic extraction reagents, Pierce BCA Protein Assay Kits, TRIzol reagent and Lipofectamine RNAiMAX were purchased from Thermo Fisher Scientific (Waltham, MA). Control siRNA (nonsilencing), EZH2 siRNA, ERK2 siRNA or TNFR2 siRNA were purchased from Santa Cruz (Santa Cruz, CA). SB203580 and U0126 were from Alexis Biochemicals (San Diego, CA). 4',6-Diamidino-2-phenylindole (DAPI) and Hoechst 33258 were purchased from Yeasen (Shanghai, China). An immunoprecipitation kit was purchased from Invitrogen (Carlsbad, CA). PrimeScript RT Master Mix and SYBR Premix Ex Taq TM were purchased from Takara (Shiga, Japan). Fluorescein isothiocyanate (FITC)-dextran and other reagents unless noted were purchased from Sigma Chemical Co. (St. Louis, MO).

Cell culture

Human mammary microvascular endothelial cells (HMMECs) and human umbilical vein endothelial cells (HUVECs) were purchased from ScienCell and cultured in endothelial cell medium (ScienCell) supplemented with 5% [*v/v*] fetal bovine serum and 1% endothelial cell growth supplement, 100 U/mL penicillin and 100 mg/mL streptomycin. MDA-MB-231-luc-GFP and 4T1-luc-GFP dual-labeled cell lines were purchased from Zhong-Qiao-Xin-Zhou Biotechnology. 4T1 (ATCC) and 4T1-luc-GFP cells were cultured in RPMI-1640 (Life Technology). MDA-MB-231 (ATCC) and MDA-MB-231-luc-GFP cells were cultured in DMEM high glucose medium (Life Technology). DMEM and RPMI 1640 medium were supplemented with 10% fetal bovine serum, 100 U/mL penicillin and 100 mg/mL streptomycin. Cells were incubated in a humidified atmosphere of 5% CO₂ at 37 °C.

Natural compound

SC (purity \geq 98.0%) was purchased from Shanghai Tauto Bio-Tech Co., Ltd. The chemical structure of SC is shown in Supplementary Fig. 1a.

Animals and treatment

Twenty-two nude (Balb/c) female mice (4 weeks old) and 47 normal Balb/c female mice (4 weeks old) were purchased from Shanghai Laboratory Animal Center of Chinese Academy of Sciences (Shanghai, China). Animals were housed under specific pathogen-free conditions according to the guidelines of the association for Assessment and Accreditation of Laboratory Animal Care. All animals received humane care according to the institutional animal care guidelines approved by the Experimental Animal Ethical Committee of Shanghai University of Traditional Chinese Medicine, and all the experimental protocols were carried out in accordance with the approved guidelines.

Animals were anaesthetized with isoflurane. Then, MDA-MB-231-luc-GFP cells (1×10^6 per mouse) were injected subcutaneously into the fourth right mammary fat pad at the base of the nipple of 17 mice with 50% matrigel (BD Biosciences). When the tumor was visible (4th week), these mice were randomly divided into three groups: (1) TNBC model ($n = 5$); (2) TNBC + SC (1 mg/kg) ($n = 5$); and (3) TNBC + SC (10 mg/kg) ($n = 5$). Two mice that failed to bear tumors were euthanized by the CO₂ asphyxiation procedure. The number of mice in the blank group without MDA-MB-231-luc-GFP cell injection was also 5. At 1 month after TNBC injection, mice were given SC (1, 10 mg/kg, intragastric administration, *i.g.*) consecutively for 2 months. The blank group and TNBC model group were treated with an equal volume of vehicle (0.5% CMC-Na in water).

Animals were anaesthetized with isoflurane, and then 4T1-luc-GFP cells (1×10^6 per mouse) were injected subcutaneously into the fourth right mammary fat pad at the base of the nipple of 40 Balb/c female mice with 50% matrigel. When the tumor was visible (\sim 7 days), three mice that failed to bear the tumor were euthanized by the CO₂ asphyxiation procedure. Twenty-one mice were used to observe TNBC metastasis and collect tissue samples. These mice were randomly divided into three groups: (1) TNBC model ($n = 7$); (2) TNBC + SC (1 mg/kg) ($n = 7$); and (3) TNBC + SC (10 mg/kg) ($n = 7$). The number of mice in the blank group without injection of 4T1-luc-GFP cells was also 7. The other sixteen mice were used to detect the permeability of vessels in primary tumors. These mice were randomly divided into two groups: (1) TNBC model ($n = 8$) and (2) TNBC + SC (10 mg/kg) ($n = 8$). At 1 week after TNBC injection, mice were given SC (1, 10 mg/kg, intragastric administration, *i.g.*) consecutively for 5 weeks. The blank group and TNBC model group were treated with an equal volume of vehicle (0.5% CMC-Na in water).

Mice were imaged to detect metastasis once every week from 11 weeks (in nude mice) or 5 weeks (in normal Balb/c) after the injection of TNBC cells. After inhalation anesthesia with isoflurane, mice were imaged by using the IVIS Lumina system with Living

Image software 4.0 (PerkinElmer) immediately after intraperitoneal injection of 2.5 mg luciferin (PerkinElmer). The total signal per defined region of interest was calculated as photons/second/cm² (total flux/area). Mice were anaesthetized by inhalation isoflurane, blood samples were taken from the abdominal aorta, and then anaesthetized mice were killed by cervical dislocation. Primary tumors and organs were harvested, paraffin-embedded, sectioned and stained with haematoxylin and eosin (H&E).

H&E staining

Lungs and livers were fixed in 4% paraformaldehyde. Samples were subsequently sectioned (5 µm), stained with H&E, and then observed under a light microscope (Olympus) to quantify the number of metastatic lesions. Enumeration was performed by counting the number of lesions regardless of size.

Detecting circulating tumor cells (CTCs) in vivo

Peripheral blood mononuclear cells (PBMCs) were isolated by the established procedure [26]. Briefly, after anesthesia, 200 µL whole blood samples were collected from the vena cava inferior of each animal into K₃-EDTA-coated tubes and treated with red blood cell lysis buffer (eBioscience) within 2 h of collection, followed by incubation at room temperature for 5 min and then pelleting the remaining blood cells at 300 g for 10 min. PBMCs were then washed twice with 1× phosphate buffer saline (PBS) and used for fluorescence labeling followed by flow cytometry (Beckman Coulter). GFP⁺ cells in PBMCs were identified as CTCs. Data generated by flow cytometry were analyzed by CytExpert software (Beckman Coulter).

In vivo vascular permeability assay

For the Evans blue leakage assay, 4T1-luc-GFP orthotopic Balb/c mice received an intraperitoneal injection of 2% Evans blue dye (in PBS, 10 µL/g) (*n* = 5/group). Two hours later, the mice were euthanized and perfused with normal saline through the left ventricle. Tumors were collected and cut into pieces of ~100 mg/piece and then incubated with formamide (4 µL/mg of tissue) at 37 °C for 24 h. After centrifugation (10,000 × *g*, 10 min), the supernatant of each tube was carefully collected and measured at 620 nm. The concentration of Evans blue dye in extracts was calculated by using a standard curve of Evans blue in formamide and normalized to the dried tumor weight.

For the FITC-dextran leakage assay, 100 µL of 70 kDa FITC-dextran (in PBS) was administered intravenously at a dose of 200 mg/kg from the tail vein of 4T1-luc-GFP orthotopic Balb/c mice (*n* = 3/group). Thirty minutes later, the animals were euthanized and perfused with normal saline through the left ventricle. Tumors were extracted, embedded in OCT and cut into 6 µm-thick sections. Fluorescence images were captured by using an Olympus IX81 inverted fluorescence microscope at different areas in three tumor samples per group.

Immunofluorescence staining assay

Paraffin-embedded sections of tumors (5 µm) were deparaffinized in xylene and then rehydrated in an ethanol gradient with distilled water. Slices were incubated with 5% bovine serum albumin (BSA) to minimize nonspecific binding. After rinsing three times, slices were incubated with VE-cadherin or α-SMA and CD31 antibodies at 4 °C overnight and further incubated with Alexa Fluor 488 goat anti-mouse IgG (H + L) antibody and Alexa Fluor 568 goat anti-rabbit IgG (H + L) antibody at room temperature for 1 h. After rinsing three times again, slices were incubated with Hoechst 33258 for 10 min. Images were captured under an inverted microscope (Olympus).

For staining VE-cadherin in HMMECs or HUVECs, cells were pretreated with or without SC (5, 20 M) for 3 h and then incubated with or without TNFα (10 ng/ml) for 24 h. For staining F-actin/VE-cadherin in HMMECs, cells were incubated with or

without TNFα (10 ng/ml) for 24 h. After treatment, cells were fixed with 4% paraformaldehyde for 30 min and then incubated with 0.3% Triton X-100 for 10 min and further blocked with 1% BSA for 1 h. Cells were probed with an appropriate combination of primary antibody (overnight at 4 °C) and Alexa Fluor 647 phalloidin- or Alexa 488-labeled goat anti-rabbit antibody or Alexa 488-labeled goat anti-mouse antibody or Alexa 568-labeled goat anti-rabbit antibody (1 h avoiding light at room temperature). Hoechst 33258 or DAPI was added to the cells to stain the nucleus for 10 min. Fluorescence photographs were captured by using an Olympus IX81 inverted fluorescence microscope.

Tumor vessel isolation

Vessels in primary mammary tumors of mice were prepared according to a previously reported method [27]. In brief, tumor tissues were dissected and homogenized in capillary buffer (10 mM HEPES, 141 mM NaCl, 4 mM KCl, 2.8 mM CaCl₂, 1 mM NaH₂PO₄, 1 mM MgSO₄, 10 mM D-glucose, pH 7.4) with Dounce glass homogenizers. The homogenate was mixed thoroughly with 26% dextran and centrifuged at 9000 × *g* for 30 min at 4 °C. The pellet with the enriched endothelial fraction was washed with PBS and then stored at –80 °C for further analysis.

Protein extraction and Western blot analysis

Cellular and tumor vascular proteins were homogenized in ice-cold lysis buffer as previously described [28]. Cytosolic and nuclear proteins were isolated as described in nuclear and cytoplasmic extraction kits. The protein concentrations were measured, and all the samples in the same experiment were normalized to equal protein concentrations.

Protein samples were separated by SDS-PAGE, transferred onto a PVDF membrane, and then incubated with the appropriate combination of primary and secondary antibodies. Proteins were visualized by using a chemiluminescent kit. The gray densities of the protein bands were normalized by using β-actin or Lamin B1 density as internal controls, and the results were further normalized to the control.

Enzyme-linked immunosorbent (ELISA) assay

The supernatants from tissue homogenate were collected at 3000 × *g* and 4 °C for 10 min for ELISA according to the manufacturer's instructions (R&D Systems). In brief, 100 µL of standard, control or sample was added to each well. The system was incubated at room temperature for 2 h. Then, each well was aspirated and washed with wash buffer (400 µL), and this process was repeated four times. Next, 100 µL of conjugate was added to each well and incubated at room temperature for 2 h. The aspiration and wash process was repeated five times. Then, 100 µL of substrate solution was added to each well and incubated at room temperature for 30 min. Then, 100 µL of Stop solution was added to each well. Finally, the optical density of each well was determined by using a microplate reader set to 450 nm.

Transendothelial electrical resistance (TEER) assay

HMMECs or HUVECs (2 × 10⁴ cells/well) were seeded into Transwell inserts (Costar, 0.4 µm). The culture medium was replaced every other day, and cells were cultured for an additional 3 to 4 days until a confluent monolayer was formed. HMMECs or HUVECs were stimulated with or without TNFα (10 ng/mL) for the indicated times. Otherwise, HMMECs or HUVECs were pretreated with or without SC (5, 20 M) for 3 h or inhibitors for 15 min and then incubated with or without TNFα (10 ng/mL) for the additional indicated time. In total, 0.1% BSA was used as a solvent control. The TEER value of the monolayer was measured at 6 h or 24 h after TNFα stimulation as previously described by using a Millicell ERS-2 volt-ohm meter (Millipore). The TEER value was calculated according to the manufacturer's instructions: TEER of the

monolayer ($\Delta\Omega\text{cm}^2$) = (sample-well resistance-blank-well resistance) area of the cell monolayer. Blank wells were transwell inserts without ECs.

FITC-conjugated dextran cell permeability assay

HMMECs or HUVECs (2×10^4 cells/well) were seeded into Transwell inserts (Costar, 8 μM). The culture medium was replaced every other day, and cells were cultured for an additional 3 to 4 days until a confluent monolayer was formed. HMMECs or HUVECs were stimulated with or without TNF α (10 ng/ml) for the indicated times. Otherwise, HMMECs or HUVECs were pretreated with or without SC (5, 20 M) for 3 h or inhibitors for 15 min and then incubated with or without TNF α (10 ng/ml) for the additional indicated time. After treatment, the leakage of FITC-dextran was detected and calculated as previously described [28].

Transendothelial migration assay

HMMECs or HUVECs (2×10^4 cells/well) were plated and allowed to reach confluence on Transwell filters (8- μm pore size; Costar). HMMECs or HUVECs were pre-incubated with or without inhibitors for 15 min or SC (5, 20 μM) or 3 h and then incubated with TNF α (10 ng/ml) for an additional 24 h. The old medium was discarded, and MDA-MB-231-luc-GFP or 4T1-luc-GFP cells were seeded into Transwell inserts at 5×10^4 cells per well. After 24 h, cells were fixed with 4% paraformaldehyde solution in PBS for 30 min, and Hoechst 33258 was added to cells to stain the nucleus for 10 min. Cells on the inner side of inserts were scraped off, and the Transwell filters were examined under an Olympus IX81 inverted fluorescence microscope to observe the migrated cells. At least three fields were randomly selected. The migration of MDA-MB-231-luc-GFP cells was quantified by counting the green fluorescence on the bottom of the Transwell in each field by ImageJ software (National Institutes of Health).

Real-time PCR assay

Cellular and tumor vessel total RNA was isolated by using TRIzol reagent according to the manufacturer's instructions. The RNA content was determined by measuring the optical density at 260 nm. Synthesis of cDNA and real-time PCR were performed as described in the PrimeScript RT Master Mix kit and SYBR Premix Ex Taq kit. The relative expression of target genes was normalized to actin. The results were analyzed by the $2^{-\Delta\Delta\text{Ct}}$ method and are given as ratios compared with the control. The primer sequences used in this study are shown in Supplementary Table 1.

siRNA transfection

Control siRNA (nonsilencing), EZH2 siRNA, ERK2 siRNA or TNFR2 siRNA were transfected into cells by using Lipofectamine RNAiMAX. The siRNA sequences are shown in Supplementary Table 2. At 24 h after transfection, cells were incubated with TNF α for an additional 24 h and then collected for further experiments, including real-time PCR, Western blot, FITC-conjugated dextran cell permeability assay and transendothelial migration assay.

Immunoprecipitation assay

HUVECs were pretreated with or without SC (20 μM) for 30 min and then incubated with TNF α (100 ng/mL) for another 30 min. Next, cells were collected and lysed in 1 \times RIPA buffer containing protease inhibitors on ice for 2 h. Cells were centrifuged, and the supernatant was collected and incubated with Dynabeads and TNFR2 antibody with gentle rocking for 30 min at room temperature. After precipitation, the Dynabeads were washed three times with cold wash buffer, boiled with 60 μL of 2 \times loading buffer for 10 min at 99 $^\circ\text{C}$ and further analyzed by Western blotting.

Statistical analysis

Data are expressed as the mean \pm standard error of the mean. SPSS 18.0 software (SPSS inc.) was used to analyze the results.

The significance of differences between groups was evaluated by one-way ANOVA with the LSD *post hoc* test, and $P < 0.05$ was considered to indicate statistically significant differences. Significant differences were marked as * $P < 0.05$, ** $P < 0.01$, *** $P < 0.001$ or # $P < 0.05$, ## $P < 0.01$, ### $P < 0.001$. The correlations in the gene expression levels were analyzed by Pearson's rank correlation coefficients. All in vitro experiments were repeated at least three times.

RESULTS

SC suppressed spontaneous TNBC metastasis in vivo

Suppression of TNBC metastasis by the natural compound SC in vivo was observed in MDA-MB-231-luc-GFP or 4T1-luc-GFP tumor-bearing mice by using an orthotopic (mammary fat pad) model. SC (10 mg/kg) significantly suppressed the metastasis of MDA-MB-231-luc-GFP cells in tumor-bearing mice (Fig. 1a and Supplementary Fig. 1b). The data in Fig. 1b show that metastatic MDA-MB-231-luc-GFP cells were detected in the liver, but SC (10 mg/kg) reduced the increased number of metastatic nodes in the liver. Consistently, SC (10 mg/kg) reduced the spontaneous metastasis of TNBC in 4T1-luc-GFP tumor-bearing Balb/c mice (Fig. 1c). SC (10 mg/kg) also decreased the enhanced number of metastatic nodes in both the liver and lung in 4T1-luc-GFP tumor-bearing mice (Fig. 1d). These results suggest that SC suppressed the metastasis of TNBC in vivo.

SC alleviated the TNBC-associated vascular endothelial barrier dysfunction in vivo

Considering the protective effect of SC on the cardiovascular system, we hypothesized that SC might reduce the haematogenous metastasis of TNBC in vivo. The results showed that SC (10 mg/kg) reduced the enhanced number of CTCs in PBMCs isolated from both MDA-MB-231-luc-GFP tumor-bearing nude mice and 4T1-luc-GFP tumor-bearing Balb/c mice (Fig. 2a). To determine whether the permeability of TNBC-associated vessels was enhanced, Evans blue dye leakage and FITC-dextran extravasation assays were conducted in 4T1-luc-GFP orthotopic Balb/c mice (Fig. 2b, c). Compared with the model group, SC (10 mg/kg) significantly decreased Evans blue exudation in primary tumors in vivo (Fig. 2b). Consistently, a large amount of FITC-conjugated dextran was found in primary tumor tissues from 4T1-luc-GFP tumor-bearing mice, but SC (10 mg/kg) obviously reduced this leakage (Fig. 2c).

Vascular permeability is always related to the expression of vascular endothelial junctional proteins. Breast invasive carcinoma data (BRCA) in The Cancer Genome Atlas (TCGA) indicate that the expression of VE-cadherin and CD31 was decreased in invasive breast tumors (Supplementary Fig. 2a). The data in Fig. 2d show that SC enhanced the number of VE-cadherin⁺/CD31⁺ cells in tumor tissues from MDA-MB-231-luc-GFP tumor-bearing mice. Moreover, SC also rescued the decreased expression of VE-cadherin, CD31 and claudin-1 in tumor vessels isolated from both MDA-MB-231-luc-GFP tumor-bearing mice and 4T1-luc-GFP tumor-bearing mice (Fig. 2e). α -SMA is commonly used as a marker for pericytes, and the coverage of pericytes to vessels indicates the maturation and normalization of vessels [29]. The results of immunohistochemistry staining showed that the number of α -SMA⁺/CD31⁺ cells in tumor tissues from the SC-treated group was higher than that in tumor tissues from the model group without SC treatment, indicating that SC promoted the normalization of tumor vessels (Supplementary Fig. 2b).

TCGA data showed that TNF α was highly expressed in TNBC patients compared with normal tissue or luminal subtypes (Fig. 2f). However, SC did not reduce the increased TNF α content in tumor tissues from either MDA-MB-231-luc-GFP tumor-bearing mice or 4T1-luc-GFP tumor-bearing mice (Fig. 2g).

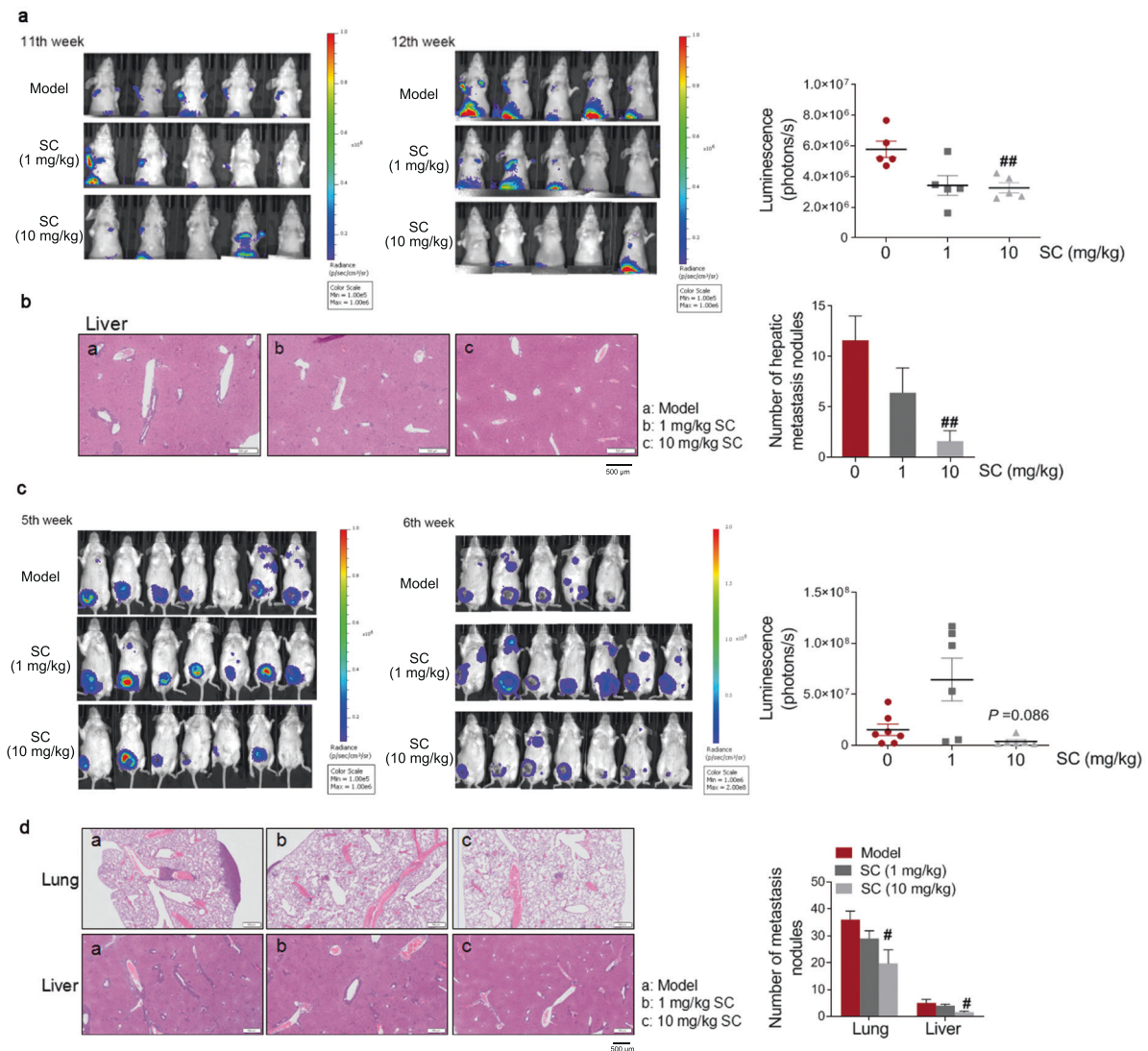


Fig. 1 SC suppressed spontaneous TNBC metastasis in vivo. **a, b** MDA-MB-231-luc-GFP cells were injected into the No. 4 mammary fat pad of nude mice. **a** Representative images of bioluminescence imaging (BLI) at 11 or 12 weeks after the injection of MDA-MB-231-luc-GFP cells. Statistical analysis of migrated area photon flux is shown right ($n = 5$). **b** Representative images of H&E staining of liver. Scale bars: 500 μm . Quantification of metastatic nodes is shown right ($n = 5$). **c, d** 4T1-luc-GFP cells were injected into the No. 4 mammary fat pad of Balb/c mice. Two mice were dead at 6th week due to the extensive tumor burden. **c** Representative images of BLI at 5 or 6 weeks after the injection of 4T1-luc-GFP cells. Statistical analysis of migrated area photon flux is shown right ($n = 5-7$). **d** Representative images of H&E staining of lung and liver. Scale bars: 500 μm . Quantification results of metastatic nodes in lung and liver are shown right ($n = 7$). Data = Mean \pm SEM. # $P < 0.05$, ## $P < 0.01$ versus model.

SC rescued TNF α -induced endothelial barrier dysfunction and transendothelial migration in TNBC in vitro. Based on the breakdown of the vascular barrier in TNBC primary tumors, we next assessed whether TNF α can induce endothelial barrier dysfunction in vitro. The data in Fig. 3a show that TNF α (10 ng/mL) decreased the expression of VE-cadherin, occludin and PECAM-1/CD31 in both HMMECs and HUVECs when cells were incubated with TNF α (10 ng/mL) for the indicated times. TGF β (10 ng/mL) also decreased the expression of VE-cadherin, occludin and CD31 in both HMMECs and HUVECs. Moreover, the results from immunofluorescence staining showed that TNF α decreased the expression of VE-cadherin and induced disorder of the cell monolayer TJ structure in HMMECs (Supplementary Fig. 3a). SC (20 μM) rescued the TNF α -induced decrease in the cellular expression of VE-cadherin, CD31 and occludin in both HMMECs and HUVECs (Fig. 3b). The results of immunofluorescence staining showed that SC (5 and 20 μM) enhanced the TNF α -induced reduction in VE-cadherin expression in both HMMECs and HUVECs

(Fig. 3c). Moreover, SC (5, 20 μM) rescued the decrease in the TEER value when HMMECs and HUVECs were incubated with TNF α for 6 or 24 h (Fig. 3d). SC (5, 20 μM) also reduced the elevated FITC-dextran leakage through an endothelial monolayer composed of TNF α -stimulated HMMECs or HUVECs (Fig. 3e). Additionally, SC (20 μM) also suppressed the elevated transendothelial migration of MDA-MB-231-luc-GFP cells (Fig. 3f) and 4T1-luc-GFP cells (Supplementary Fig. 3b, c) through an endothelial monolayer composed of TNF α -stimulated HMMECs or HUVECs.

EZH2 was involved in the TNF α -induced transendothelial migration of TNBC. As previous studies reported, EZH2 is a classical transcription repressor regulating the expression of some junctional proteins in ECs [30, 31]. From the TCGA data, we found that the TNF α level was closely associated with the expression of EZH2 (Fig. 4a). As shown in Fig. 4b, TNF α (10 ng/mL) enhanced the nuclear accumulation of EZH2 in both HMMECs and HUVECs. According to the analysis of

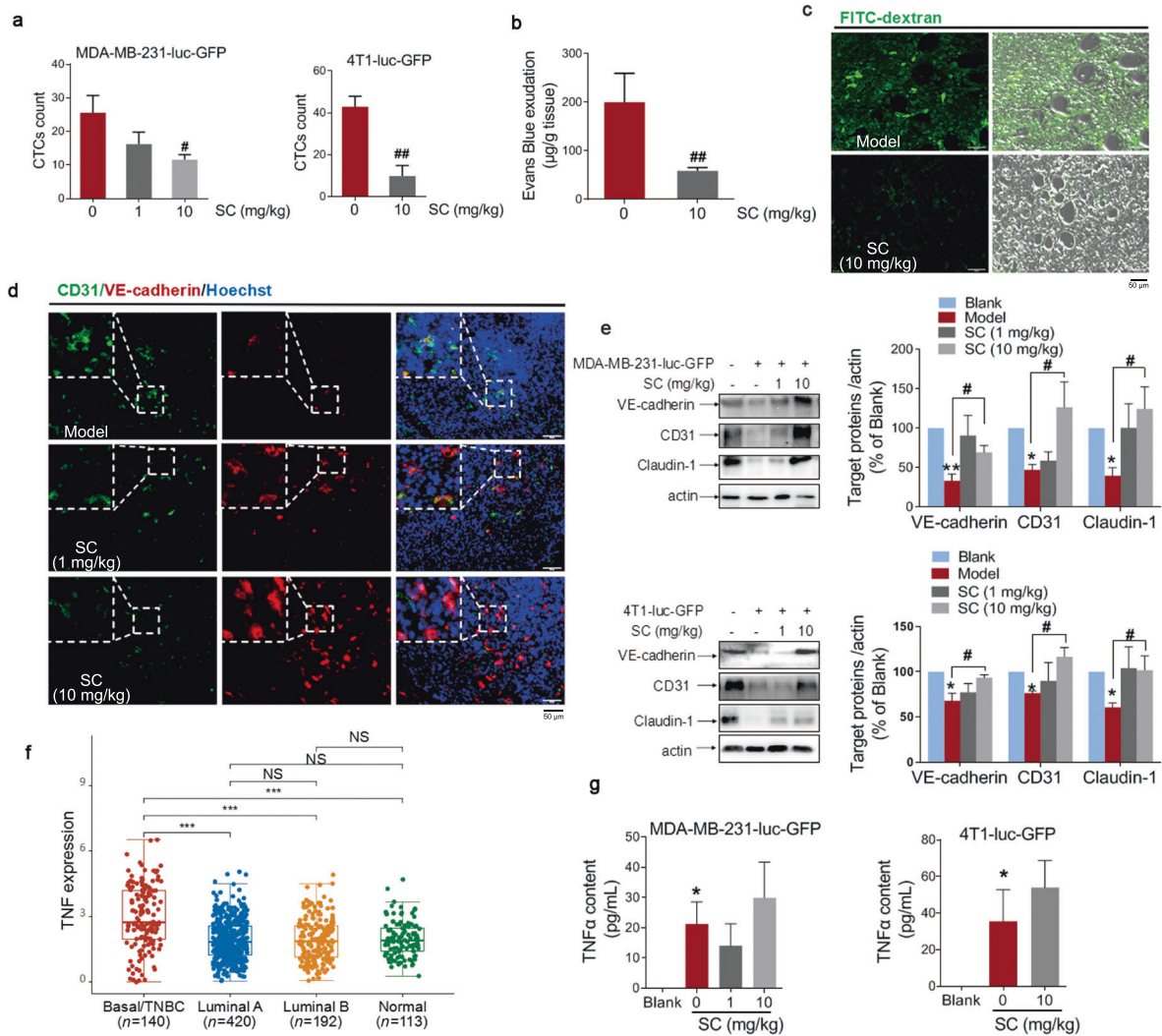


Fig. 2 SC alleviated the TNBC-associated vascular endothelial barrier dysfunction in vivo. **a** CTC numbers were analyzed by flow cytometry in MDA-MB-231-luc-GFP bearing nude mice ($n = 5$) and 4T1-luc-GFP bearing Balb/c normal mice ($n = 5$). **b** Primary tumor vascular leakage was measured by Evans blue assay in 4T1-luc-GFP bearing Balb/c normal mice ($n = 5$). **c** Representative images of 70-kDa FITC-dextran (green) extravasation in primary tumor from 4T1-luc-GFP bearing Balb/c normal mice ($n = 3$, scale bar: 50 μm). **d** Representative immunofluorescence image of CD31 and VE-cadherin-stained MDA-MB-231-luc-GFP tumor section ($n = 5$, scale bar: 50 μm). **e** Representative image (left) and quantification (right) of VE-cadherin, claudin-1 and CD31 expression in tumor vessels isolated from MDA-MB-231-luc-GFP bearing nude mice ($n = 5$) and 4T1-luc-GFP bearing Balb/c normal mice ($n = 5$). **f** TNF α mRNA expression in tumor or normal tissues from TCGA data of BRCA (Kruskal–Wallis test $P = 1.9 \times 10^{-14}$). **g** TNF α content in tumor tissues from MDA-MB-231-luc-GFP ($n = 5$) or 4T1-luc-GFP bearing mice ($n = 5$). Data = Mean \pm SEM. * $P < 0.05$, ** $P < 0.01$, *** $P < 0.001$ versus control; # $P < 0.05$, ## $P < 0.01$ versus model; NS indicates no significant differences.

TCGA-BRCA data, the expression of VE-cadherin and CD31 had a negative correlation with EZH2 expression (Supplementary Fig. 4a). Next, EZH2 chemical inhibitor GSK126 was used. GSK126 rescued the downregulated cellular mRNA (Fig. 4c) and protein (Fig. 4d) expression of VE-cadherin, occludin and CD31 induced by TNF α in both HMMECs and HUVECs. Moreover, GSK126 obviously rescued the TNF α -induced decrease in the TEER value (Fig. 4e) and increase in FITC-dextran leakage (Fig. 4f) in endothelial monolayers formed by HMMECs or HUVECs. Additionally, GSK126 reduced the elevated transendothelial migration of MDA-MB-231-luc-GFP cells through an endothelial monolayer formed by TNF α -stimulated HMMECs or HUVECs (Fig. 4g).

ERK1/2 was involved in the TNF α -induced transendothelial migration of TNBC

Next, we explored the upstream signal regulating EZH2 activation. As shown in Fig. 5a, the phosphorylation of ERK1/2 and p38 was obviously increased upon TNF α (10 ng/mL)

stimulation in a time-dependent manner. U0126 (ERK1/2 chemical inhibitor) rescued the decreased expression of VE-cadherin in TNF α -stimulated HMMECs, but SB203580 (p38 chemical inhibitor) did not have this effect (Fig. 5b). In addition, U0126 and ERK2 siRNA (the expression of ERK2 in cells transfected with ERK2 siRNA is shown in Supplementary Fig. 4b) both decreased the enhanced nuclear accumulation of EZH2 induced by TNF α in HMMECs (Fig. 5c, d). Moreover, both ERK2 and EZH2 siRNA (the expression of EZH2 in cells transfected with EZH2 siRNA is shown in Supplementary Fig. 4b) rescued the decreased cellular expression of VE-cadherin, occludin and CD31 induced by TNF α in HMMECs (Fig. 5e). Additionally, U0126 also decreased the elevated EZH2 nuclear accumulation and rescued the reduced expression of VE-cadherin, occludin and CD31 induced by TNF α in HUVECs (Fig. 5f). Moreover, U0126 reduced the enhanced transendothelial migration of MDA-MB-231-luc-GFP cells through the confluent monolayer formed by TNF α -stimulated HMMECs or HUVECs (Fig. 5g).

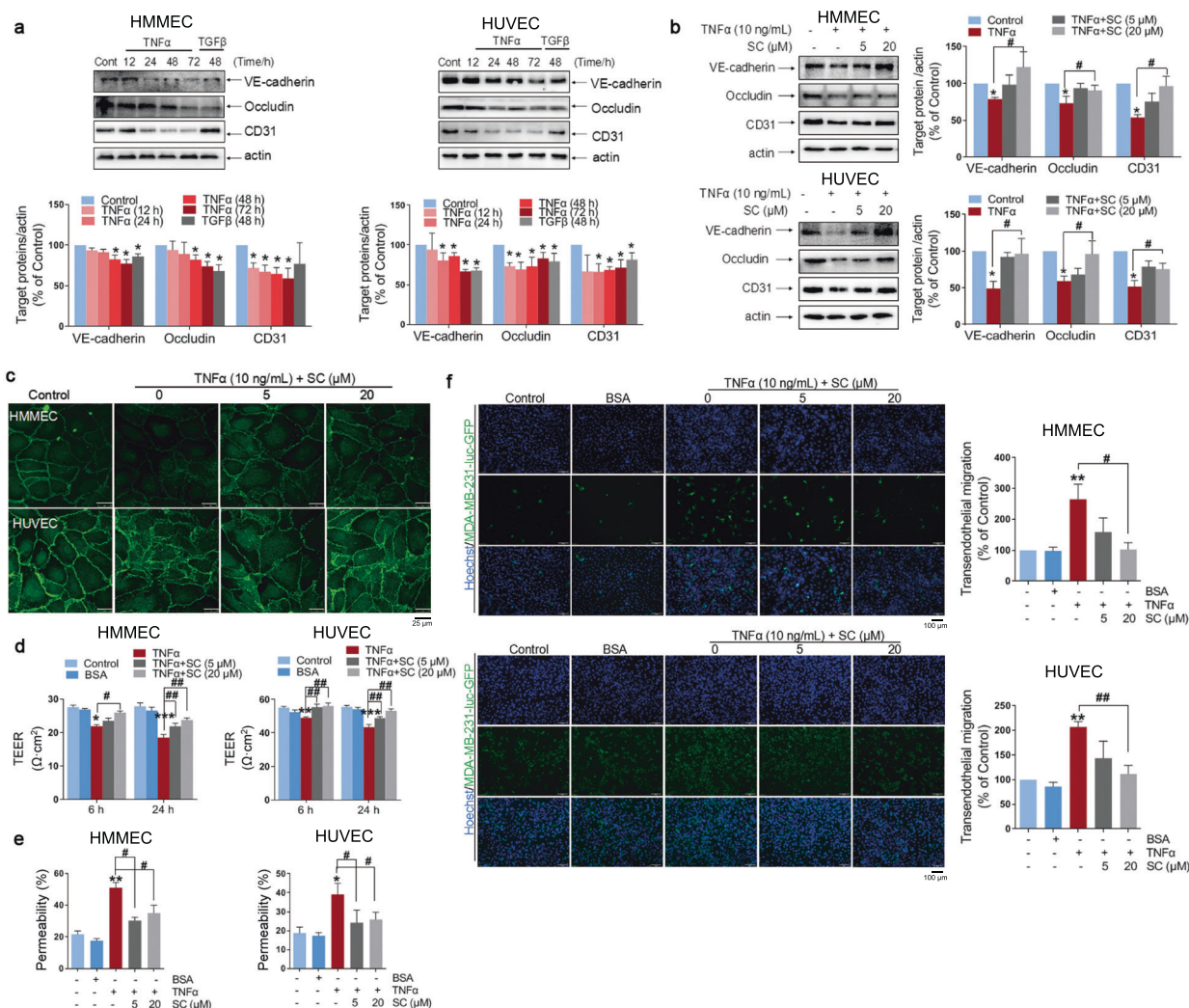


Fig. 3 SC rescued the TNF α -induced endothelial barrier dysfunction in vitro. **a** HMMECs ($n = 3-4$) or HUVECs ($n = 3-4$) were incubated with TNF α (10 ng/mL) or TGF β (10 ng/mL) for the indicated time. Representative image (upper) and quantification (lower) of cellular VE-cadherin, occludin and CD31 expression. **b-e** HMMECs or HUVECs were pretreated with or without SC (5, 20 μ M) for 3 h, and then incubated with TNF α (10 ng/mL) for another 24 h. **b** Representative image (left) and quantification (right) of VE-cadherin, occludin and CD31 expression in HMMECs ($n = 3-4$) or HUVECs ($n = 3-4$). **c** Representative immunofluorescence images of VE-cadherin-stained HMMECs or HUVECs monolayer (scale bar: 25 μ m), and the results represent three repeated experiments. **d** The TEER value of HMMECs ($n = 3$) or HUVECs monolayer ($n = 3$). **e** FITC-dextran leakage through HMMECs ($n = 3$) or HUVECs monolayer ($n = 3$). **f** Transendothelial migration of MDA-MB-231-luc-GFP cells through endothelial monolayer composed of HMMECs ($n = 3$) or HUVECs ($n = 3$). Representative image (left, scale bar: 100 μ m) and quantification (right). Data = Mean \pm SEM. * $P < 0.05$, ** $P < 0.01$, *** $P < 0.001$ versus control; # $P < 0.05$, ## $P < 0.01$ versus TNF α .

TNFR2 played a critical role in the TNF α -induced transendothelial migration of TNBC

Next, we analyzed whether TNFR1 or TNFR2 was involved in the TNF α -induced transendothelial migration of TNBC. As shown in Supplementary Fig. 5a, R-7050 (an inhibitor of TNFR1) did not inhibit the transendothelial migration of MDA-MB-231-luc-GFP cells through an endothelial monolayer formed by TNF α -stimulated HMMECs or HUVECs. Additionally, TNF α also had no obvious cytotoxicity in either HUVECs or HMMECs (Supplementary Fig. 5b). The results of Hoechst staining suggested that stimulation with TNF α (10 ng/mL) at 6, 12, or 24 h did not cause cell apoptosis in either HMMECs or HUVECs (Supplementary Fig. 5c).

TNFR2 siRNA was further used, and the knockdown of cellular expression of TNFR2 in both HMMECs and HUVECs is shown in Supplementary Fig. 5d. TNFR2 siRNA rescued the TNF α -induced decrease in the expression of VE-cadherin, CD31 and occludin in both HMMECs and HUVECs (Fig. 6a). In addition, TNF α -induced ERK1/2 phosphorylation was diminished in both HMMECs and

HUVECs transfected with TNFR2 siRNA (Fig. 6b). Next, TNF α -induced EZH2 nuclear accumulation in both HMMECs and HUVECs was also obviously reduced by TNFR2 siRNA (Fig. 6c). Further results showed that TNFR2 siRNA reduced the elevated leakage of FITC-dextran through the endothelial barrier formed by TNF α -stimulated HMMECs or HUVECs (Fig. 6d). Moreover, the lack of TNFR2 also reduced the transendothelial migration of MDA-MB-231-luc-GFP cells through a vascular monolayer formed by TNF α -treated HMMECs or HUVECs (Fig. 6e).

SC blocked the TNFR2-ERK1/2-EZH2 signaling axis both in vivo and in vitro

HMMECs or HUVECs were pretreated with or without SC (5, 20 μ M) for 3 h and then incubated with TNF α (10 ng/mL) for another 24 h. The data in Fig. 7a show that SC (20 μ M) reduced the enhanced phosphorylation of ERK1/2 induced by TNF α in both HMMECs and HUVECs. SC also reduced the phosphorylated activation of ERK1/2 in tumor vessels isolated from both MDA-MB-231-luc-GFP and

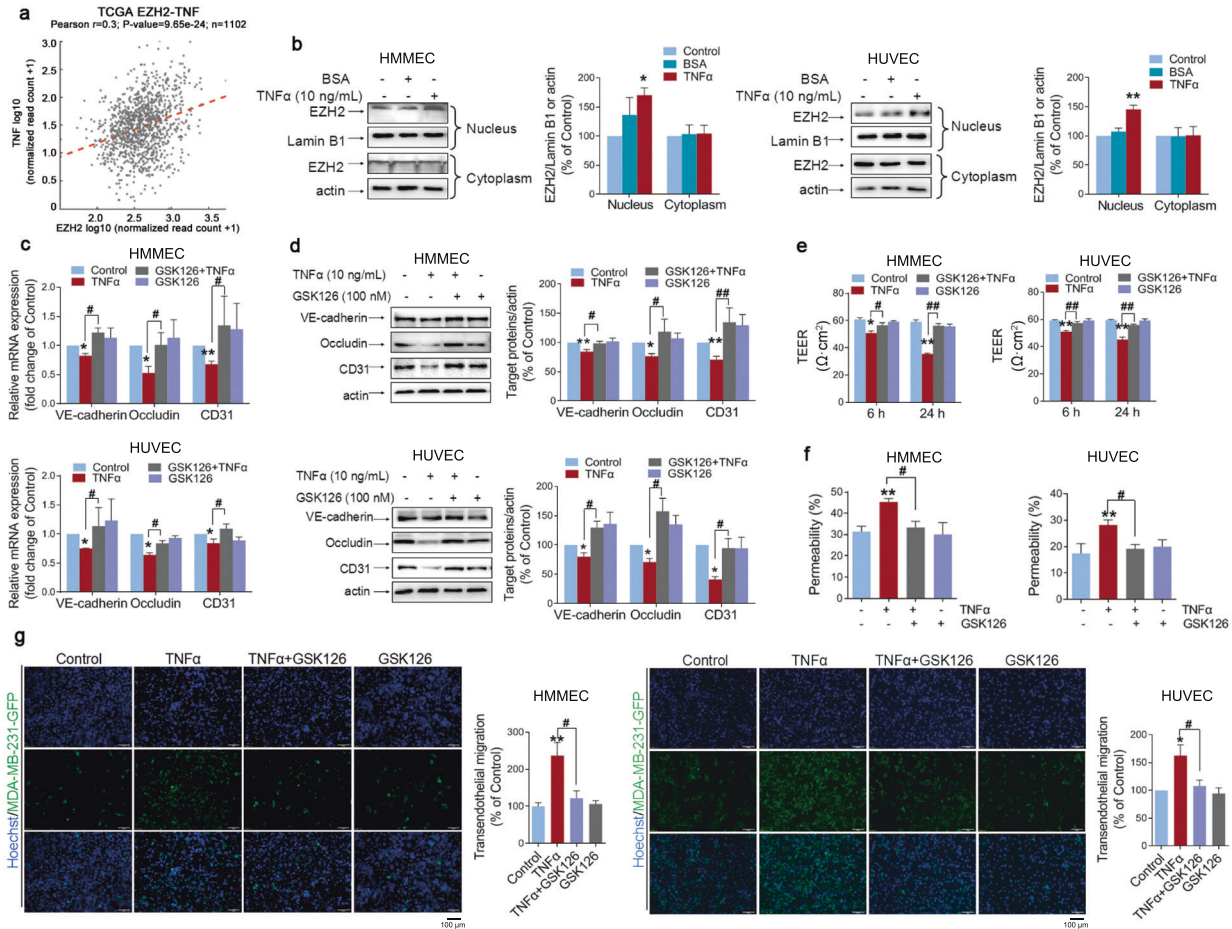


Fig. 4 EZH2 was involved in the TNF α -induced transendothelial migration of TNBC. **a** The association between the expression of EZH2 and TNF α in BRCA data from TCGA. **b** Representative image (left) and quantification (right) of the EZH2 nuclear accumulation in HMMECs ($n = 4$) or HUVECs ($n = 3-4$). **c** Cellular mRNA expression of VE-cadherin, occludin and CD31 in HMMECs ($n = 3-5$) or HUVECs ($n = 3$). **d** Representative image (left) and quantification (right) of cellular VE-cadherin, occludin and CD31 expression in HMMECs ($n = 3-6$) or HUVECs ($n = 3-4$). **e** The TEER value of HMMECs ($n = 3$) or HUVEC ($n = 3$) monolayer. **f** FITC-dextran leakage through HMMEC ($n = 3$) or HUVECs ($n = 3$) monolayer. **g** Transendothelial migration of MDA-MB-231-luc-GFP cells through endothelial monolayer composed of HMMECs ($n = 3$) or HUVECs ($n = 3$). Representative image (left, scale bar: 100 μ m) and quantification (right). Data = Mean \pm SEM. * $P < 0.05$, ** $P < 0.01$ versus control; # $P < 0.05$, ## $P < 0.01$ versus TNF α .

4T1-luc-GFP tumor-bearing mice (Fig. 7b). Additionally, SC (20 μ M) also reduced the increased accumulation of nuclear EZH2 in TNF α -stimulated HMMECs or HUVECs (Fig. 7c). Further results showed that the nuclear translocation of EZH2 was obviously enhanced in tumor vessels, but SC decreased this increase in vivo (Fig. 7d). In addition, an immunoprecipitation assay was further conducted to detect whether SC (20 μ M) can interfere with the binding of TNF α to TNFR2. The data in Supplementary Fig. 6 show that SC reduced the binding of TNF α to TNFR2 in HUVECs.

DISCUSSION

The natural compound SC has already been reported to inhibit the metastasis of many tumors (including bladder cancer, liver cancer, tongue cancer, glioma cancer, malignant melanoma cancer and colorectal cancer) mainly by inhibiting epithelial-mesenchymal transition and neoangiogenesis and inducing the degradation of extracellular matrix in the tumor microenvironment [23-25, 32-35]. Moreover, SC (80 μ M) has been found to directly inhibit the metastasis of estrogen receptor-positive MCF-7 breast cancer cells [36]. However, there is still no study about the inhibitory effect of SC on TNBC metastasis. In this study, SC was found to suppress the metastasis of TNBC in vivo for the first time. At the same time, we noticed that SC

decreased the elevated number of CTCs in PBMCs isolated from TNBC-bearing mice, indicating that SC reduced TNBC transvascular metastasis in vivo.

Previous studies found that vascular permeability enhanced cancer metastasis [37, 38]. In this study, SC suppressed Evans blue dye leakage and FITC-dextran extravasation in tumor tissues in vivo, suggesting that SC reduced vascular permeability in TNBC-associated vessels. A vascular EC monolayer composed of AJs and TJs is the final and crucial membrane barrier for the invasion of tumor cells into blood vessels [38, 39]. AJs and TJs adhere to other adhesive proteins and then form pericellular zipper-like structures among EC borders [40]. In addition, CD31 also contributes importantly to the maintenance of EC junctional integrity by combining a mechanosensory complex with VE-cadherin [41, 42]. Thus, the disruption of these junctions will lead to vascular hyperpermeability, edema and uncontrolled tension. In this study, SC rescued the decreased expression of junctional proteins, including VE-cadherin, claudin-1 and CD31, in TNBC-associated vessels. Additionally, SC also promoted the coverage of pericytes to vessels. These data suggest that SC alleviated TNBC-associated vascular endothelial barrier injury and promoted the normalization of vessels, thus abrogating TNBC transvascular metastasis in vivo.

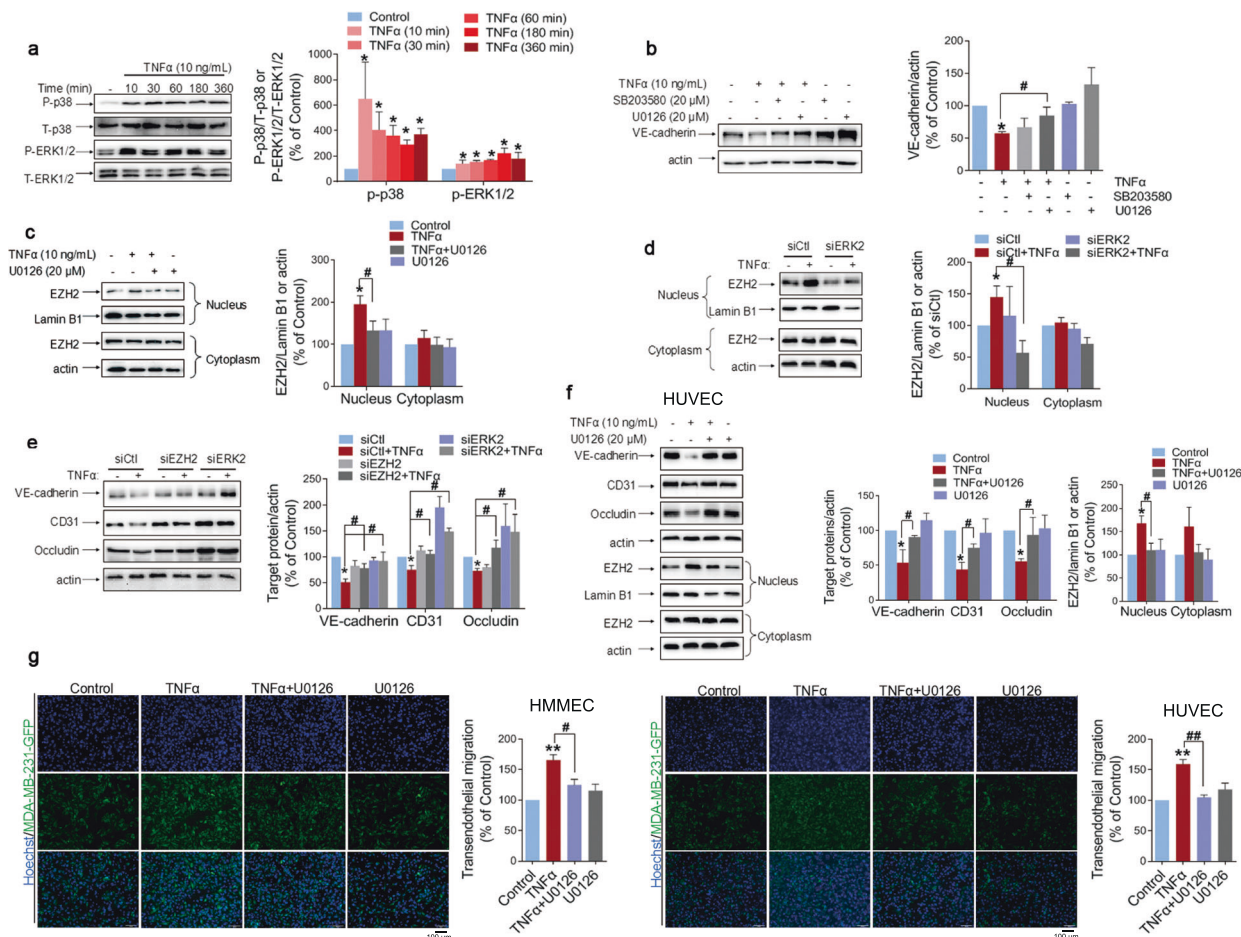


Fig. 5 ERK1/2 was involved in the TNF α -induced transendothelial migration of TNBC. **a** Representative image (left) and quantification (right) of the phosphorylation of p38 ($n = 5$) or ERK1/2 ($n = 3$) in HMMECs. **b** Representative image (left) and quantification (right) of VE-cadherin expression in HMMECs ($n = 3$). **c** Representative image (left) and quantification (right) of EZH2 nuclear accumulation in HMMECs ($n = 4-5$) after U0126 treatment. **d** Representative image (left) and quantification (right) of EZH2 nuclear accumulation in HMMECs ($n = 3$) after ERK2 siRNA transfection. **e** Representative image (left) and quantification (right) of VE-cadherin, occludin and CD31 expression in HMMECs ($n = 3$) after ERK2 siRNA transfection. **f** Representative image and quantification of VE-cadherin, occludin, CD31 expression ($n = 3$) and EZH2 nuclear accumulation ($n = 3-4$) in HUVECs after U0126 treatment. **g** Transendothelial migration of MDA-MB-231-luc-GFP cells through endothelial monolayer composed of HMMECs ($n = 3$) or HUVECs ($n = 3$). Representative image (left, scale bar: 100 μ m) and quantification (right). Data = Mean \pm SEM. * $P < 0.05$, ** $P < 0.01$ versus control; # $P < 0.05$, ## $P < 0.01$ versus TNF α .

Highly expressed TNF α is harmful to the vascular endothelium [17], but SC did not decrease the elevated TNF α content in tumor tissues. TNF α (10 ng/mL) decreased the expression of VE-cadherin, occludin and CD31 in ECs, but SC rescued the TNF α -induced decrease in those endothelial junctional proteins. Next, the results showed that SC suppressed FITC-dextran leakage, TEER decrease and TNBC transendothelial migration through an endothelial monolayer composed of TNF α -stimulated HMMECs or HUVECs. These results suggest that TNF α disrupted endothelial barrier integrity by decreasing the expression of VE-cadherin, occludin and CD31, but SC abrogated TNBC transendothelial migration by alleviating TNF α -induced endothelial barrier injury.

EZH2, the catalytic subunit of polycomb repressive complex 2 (PRC2), contributes to transcriptional silencing via the methylation of histone H3 at lysine 27 along with other PRC2 components [31]. EZH2 targeting the expression of genes, including FOXC1, β -catenin and E-cadherin, is always associated with worse progression of breast cancer [43–45]. However, the involvement of EZH2 in regulating tumor-associated vessels is less known. First, we found that TNF α induced the nuclear translocation of EZH2 in both HMMECs and HUVECs. Next, the EZH2 inhibitor GSK126 and EZH2 siRNA both rescued the downregulated expression of

junctional proteins induced by TNF α in ECs. GSK126 also alleviated endothelial barrier damage and reduced the enhanced transendothelial migration of TNBC through a vascular endothelial monolayer formed by TNF α -stimulated HMMECs or HUVECs. These results imply that EZH2 plays a crucial role in TNF α -induced vascular barrier disruption and subsequent transendothelial migration of TNBC. Finally, we also found that SC reduced the nuclear accumulation of EZH2 both in TNBC-associated vessels and in TNF α -treated ECs, implying that SC alleviated TNF α -induced vascular endothelial barrier injury by abrogating EZH2 activation.

Previous studies have shown that various kinases can induce the phosphorylation of EZH2 and subsequently regulate EZH2 activity [46, 47]. SC has already been reported to regulate the activation of ERK1/2 or p38 kinase in infarct cardiac tissue [48]. In this study, both p38 and ERK1/2 were activated in ECs after TNF α stimulation, but only the ERK1/2 chemical inhibitor U0126 restored the TNF α -induced decrease in VE-cadherin expression. The nuclear accumulation of EZH2 induced by TNF α was blocked in ECs pretreated with U0126 or transfected with ERK2 siRNA. Moreover, ERK2 siRNA rescued the reduced expression of VE-cadherin, occludin and CD31 in ECs treated with TNF α . U0126 also obviously reduced the transendothelial migration of TNBC cells through an

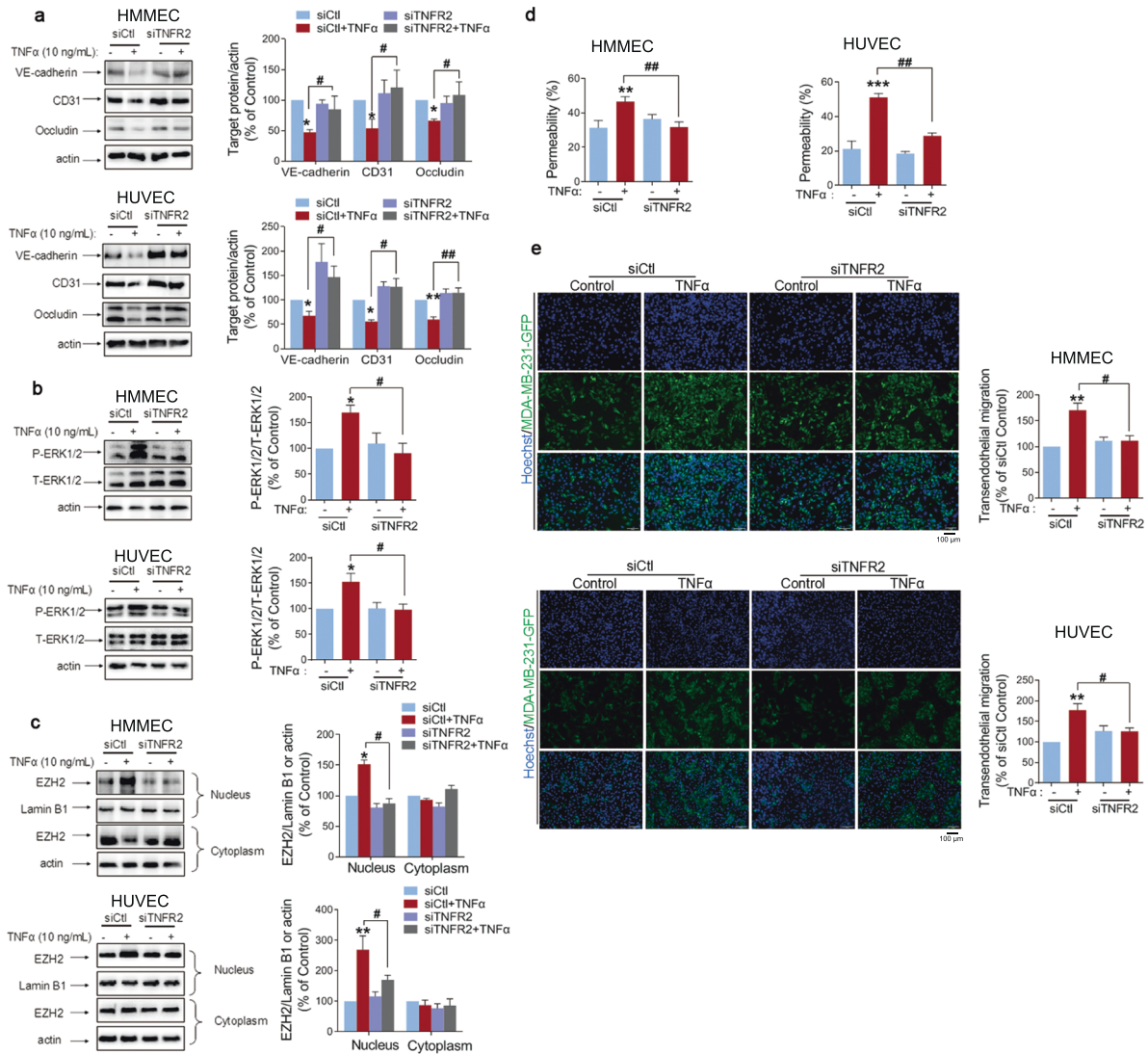


Fig. 6 TNFR2 played a critical role in the TNF α -induced transendothelial migration of TNBC. **a** Representative image (left) and quantification (right) of VE-cadherin, occludin and CD31 expression in HMMECs ($n = 3$) or HUVECs ($n = 3$). **b** Representative image (left) and quantification (right) of ERK1/2 phosphorylation in HMMECs ($n = 4$) or HUVECs ($n = 4$). **c** Representative image (left) and quantification (right) of EZH2 nuclear translocation in HMMECs ($n = 3$) or HUVECs ($n = 3-4$). **d** FITC-dextran leakage through the HMMECs ($n = 3$) or HUVECs ($n = 3$). **e** Transendothelial migration of MDA-MB-231-luc-GFP cells through endothelial monolayer composed of HMMECs ($n = 3$) or HUVECs ($n = 3$). Representative image (left, scale bar: 100 μ m) and quantification (right). Data = Mean \pm SEM. * $P < 0.05$, ** $P < 0.01$, *** $P < 0.001$ versus control; # $P < 0.05$, ## $P < 0.01$ versus TNF α .

endothelial monolayer formed by TNF α -treated HMMECs or HUVECs. All these results confirmed the important role of ERK1/2 in regulating TNF α -initiated vascular barrier disruption and the subsequent TNBC transendothelial migration, and ERK1/2 is upstream of EZH2. Moreover, SC abrogated ERK1/2 activation in both TNBC-associated vessels and TNF α -treated ECs, indicating that SC attenuated TNF α -induced vascular endothelial barrier injury by inhibiting ERK1/2-EZH2 activation.

TNFR1 and TNFR2 are two classical receptors that belong to the TNF superfamily. TNFR1 is ubiquitous in multiple types of cells and mainly participates in regulating the progression of cell death [49]. In this study, TNF α (10 ng/mL) did not cause obvious cytotoxicity or apoptosis in either HMMECs or HUVECs. Moreover, the TNFR1 inhibitor R-7050 failed to inhibit the transendothelial migration of TNBC in vitro. These results imply that the TNF α -induced transendothelial migration of TNBC is not TNFR1-dependent. TNFR2, mainly expressed in immune, endothelial and neuronal cells, is responsible for modulating cell differentiation or the immune response [50].

Recently, TNFR2 has been considered a new striking therapeutic target involved in cancer immunotherapy [49]. However, the function of TNFR2 in ECs during the progression of TNBC is still unclear. Our results showed that TNFR2 siRNA rescued the decreased expression of junctional proteins and reduced the activation of the ERK1/2-EZH2 signaling pathway induced by TNF α in ECs. Moreover, TNFR2 siRNA also decreased the elevated FITC-dextran leakage and transendothelial migration of TNBC cells. All these results imply that TNFR2 is critically involved in TNF α -triggered endothelial barrier dysfunction and thus plays an important role in the transendothelial migration of TNBC cells. Our results also showed that SC reduced the binding of TNF α to TNFR2 and thus blocked the activation of the downstream TNFR2-ERK1/2-EZH2 signaling pathway. Whether SC binds to TNF α or TNFR2 and the specific binding site need further in-depth investigation.

In conclusion, we demonstrated that TNF α -TNFR2-ERK1/2-EZH2 signaling axis-initiated vascular endothelial barrier dysfunction was critically involved in TNBC metastasis. The natural

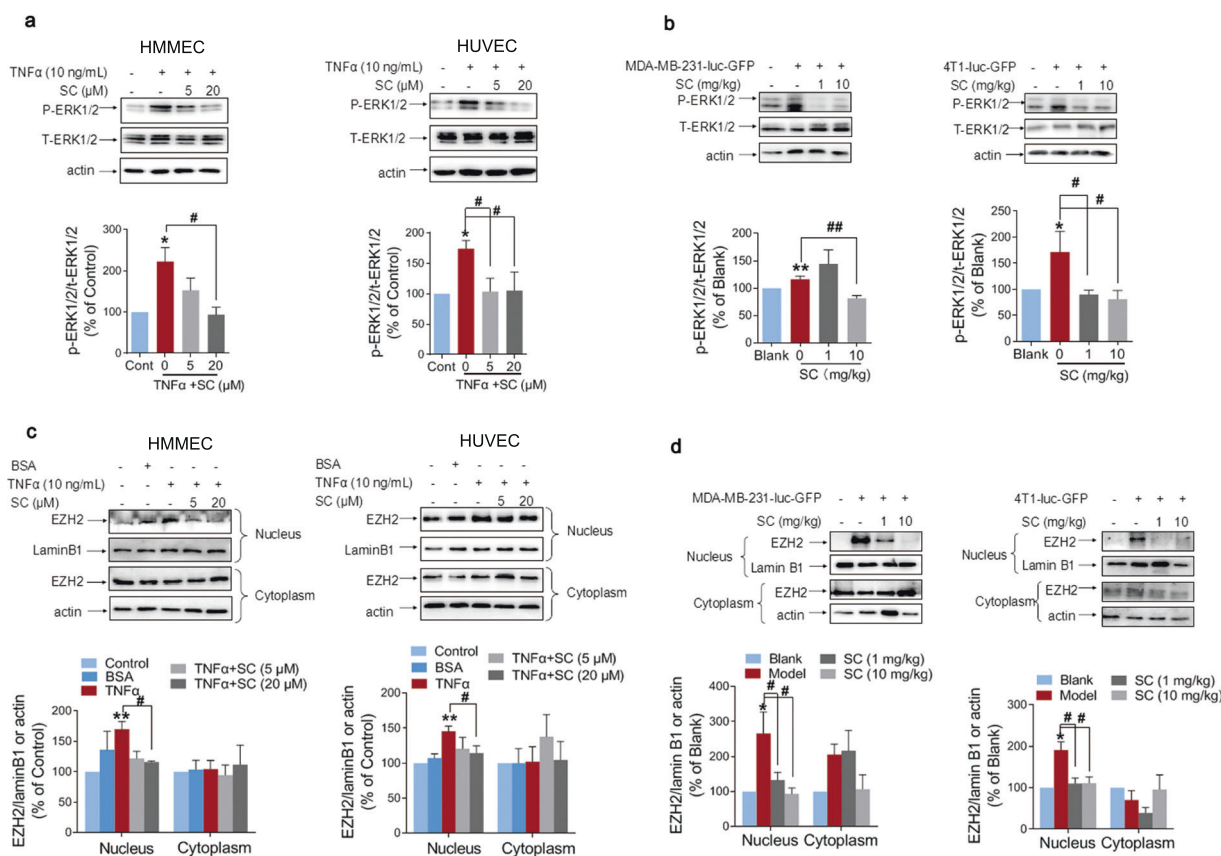


Fig. 7 SC blocked TNF-induced ERK1/2-EZH2 signaling axis both in vivo and in vitro. a Representative image (upper) and quantification (lower) of ERK1/2 phosphorylation in HMMECs ($n = 3$) and HUVECs ($n = 3$). **b** Representative image (upper) and quantification (lower) of ERK1/2 phosphorylation in tumor vessels isolated from nude ($n = 5$) and Balb/c normal ($n = 5$) mice. **c** Representative image (upper) and quantification (lower) of EZH2 nuclear accumulation in HMMECs ($n = 4$) and HUVECs ($n = 3$). **d** Representative image (upper) and quantification (lower) of EZH2 nuclear accumulation in tumor vessels isolated from nude ($n = 5$) and Balb/c normal ($n = 6-7$) mice. Data = Mean \pm SEM. * $P < 0.05$, ** $P < 0.01$ versus control; # $P < 0.05$, ## $P < 0.01$ versus TNF α .

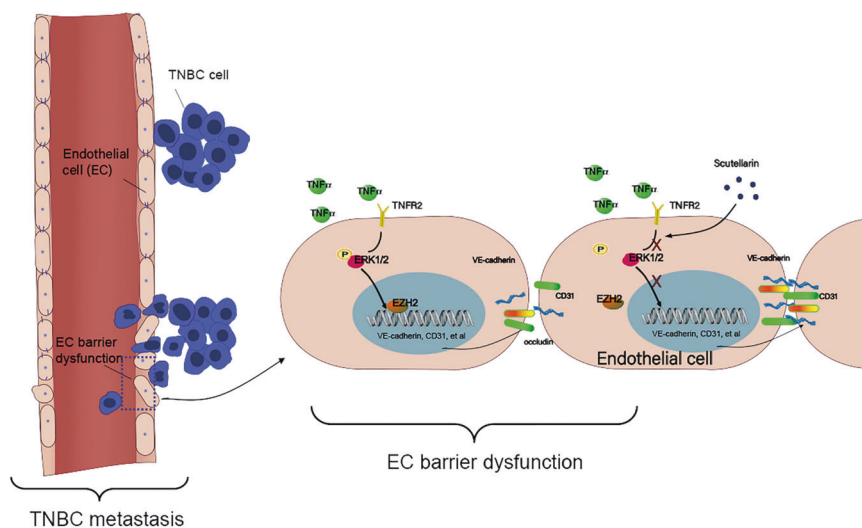


Fig. 8 A schematic presentation of process involved in the inhibitory effect of SC on TNBC metastasis. SC alleviated TNF α -induced vascular endothelial barrier dysfunction by inhibiting the TNFR2-ERK1/2-EZH2 signaling pathway in ECs, and therefore reduced TNBC metastasis.

compound SC reduced TNBC metastasis through alleviating TNF α -induced vascular endothelial barrier dysfunction by inhibiting the TNFR2-ERK1/2-EZH2 signaling pathway in ECs (Fig. 8). This study reveals a new potential therapeutic strategy by targeting aberrant vascularization for TNBC treatment.

ACKNOWLEDGEMENTS

The authors thank Prof. Zi-jia Zhang (Shanghai University of Traditional Chinese Medicine, Shanghai) for kindly gifting MDA-MB-231 cells. This work was financially supported by National Natural Science Foundation of China (82074084) and the leadership in Science and Technology innovation of the third batch of national "Ten Thousand People Plan" for LLJ.

AUTHOR CONTRIBUTIONS

XYM and LLJ conceived and designed the study; XYM, JNZ, WYJ, MHW, TYZ, and BL performed the experiments and analyzed the data; XYM drafted the manuscript; LLJ reviewed and edited the manuscript.

ADDITIONAL INFORMATION

Supplementary information The online version contains supplementary material available at <https://doi.org/10.1038/s41401-022-00873-y>.

Competing interests: The authors declare no competing interests.

REFERENCES

- DeSantis CE, Ma J, Gaudet MM, Newman LA, Miller KD, Goding Sauer A, et al. Breast cancer statistics, 2019. *CA Cancer J Clin.* 2019;69:438–51.
- Harbeck N, Gnant M. Breast cancer. *Lancet.* 2017;389:1134–50.
- Kennecke H, Yerushalmi R, Woods R, Cheang MC, Voduc D, Speers CH, et al. Metastatic behavior of breast cancer subtypes. *J Clin Oncol.* 2010;28:3271–7.
- Waks AG, Winer EP. Breast cancer treatment: a review. *JAMA.* 2019;321:288–300.
- Wu T, Dai Y. Tumor microenvironment and therapeutic response. *Cancer Lett.* 2017;387:61–8.
- Hanahan D, Weinberg RA. Hallmarks of cancer: the next generation. *Cell.* 2011;144:646–74.
- Albini A, Tosetti F, Li VW, Noonan DM, Li WW. Cancer prevention by targeting angiogenesis. *Nat Rev Clin Oncol.* 2012;9:498–509.
- Ueda S, Saeki T, Osaki A, Yamane T, Kuji I. Bevacizumab induces acute hypoxia and cancer progression in patients with refractory breast cancer: multimodal functional imaging and multiplex cytokine analysis. *Clin Cancer Res.* 2017;23:5769–78.
- Bazzoni G, Dejana E. Endothelial cell-to-cell junctions: molecular organization and role in vascular homeostasis. *Physiol Rev.* 2004;84:869–901.
- Liu Z, Wang Y, Huang Y, Kim B, Shan H, Wu D, et al. Tumor vasculatures: a new target for cancer immunotherapy. *Trends Pharmacol Sci.* 2019;40:613–23.
- Viallard C, Larrivée B. Tumor angiogenesis and vascular normalization: alternative therapeutic targets. *Angiogenesis.* 2017;20:409–26.
- Park JS, Kim IK, Han S, Park I, Kim C, Bae J, et al. Normalization of tumor vessels by Tie2 activation and Ang2 inhibition enhances drug delivery and produces a favorable tumor microenvironment. *Cancer Cell.* 2016;30:953–67.
- Andres AC, Djonov V. The mammary gland vasculature revisited. *J Mammary Gland Biol Neoplasia.* 2010;15:319–28.
- Cruceri D, Baldasici O, Balacescu O, Berindan-Neagoe I. The dual role of tumor necrosis factor- α (TNF- α) in breast cancer: molecular insights and therapeutic approaches. *Cell Oncol.* 2020;43:1–18.
- Lippitz BE. Cytokine patterns in patients with cancer: a systematic review. *Lancet Oncol.* 2013;14:e218–28.
- Egberts JH, Cloosters V, Noack A, Schniewind B, Thon L, Klose S, et al. Anti-tumor necrosis factor therapy inhibits pancreatic tumor growth and metastasis. *Cancer Res.* 2008;68:1443–50.
- Balkwill F. Tumor necrosis factor and cancer. *Nat Rev Cancer.* 2009;9:361–71.
- Madhusudan S, Foster M, Muthuramalingam SR, Braybrooke JP, Wilner S, Kaur K, et al. A phase II study of etanercept (Enbrel), a tumor necrosis factor α inhibitor in patients with metastatic breast cancer. *Clin Cancer Res.* 2004;10:6528–34.
- Kalliolias GD, Ivashkiv LB. TNF biology, pathogenic mechanisms and emerging therapeutic strategies. *Nat Rev Rheumatol.* 2016;12:49–62.
- Hu X, Li B, Li X, Zhao X, Wan L, Lin G, et al. Transmembrane TNF- α promotes suppressive activities of myeloid-derived suppressor cells via TNFR2. *J Immunol.* 2014;192:1320–31.
- Commission CP. Pharmacopoeia of the People's Republic of China (2020 version). Beijing: The Medicine Science and Technology Press of China; 2020. p. 872–1110.
- Gao J, Chen G, He H, Liu C, Xiong X, Li J, et al. Therapeutic effects of breviscapine in cardiovascular diseases: a review. *Front Pharmacol.* 2017;8:289.
- Liu K, Tian T, Zheng Y, Zhou L, Dai C, Wang M, et al. Scutellarin inhibits proliferation and invasion of hepatocellular carcinoma cells via down-regulation of JAK2/STAT3 pathway. *J Cell Mol Med.* 2019;23:3040–4.
- Lv WL, Liu Q, An JH, Song XY. Scutellarin inhibits hypoxia-induced epithelial-mesenchymal transition in bladder cancer cells. *J Cell Physiol.* 2019;234:23169–75.
- Zhu PT, Mao M, Liu ZG, Tao L, Yan BC. Scutellarin suppresses human colorectal cancer metastasis and angiogenesis by targeting ephrinb2. *Am J Transl Res.* 2017;9:5094–104.
- Boral D, Vishnoi M, Liu HN, Yin W, Sprouse ML, Scamardo A, et al. Molecular characterization of breast cancer CTCs associated with brain metastasis. *Nat Commun.* 2017;8:196.
- Yu C, Kastin AJ, Ding Y, Pan W. Gamma glutamyl transpeptidase is a dynamic indicator of endothelial response to stroke. *Exp Neurol.* 2007;203:116–22.
- Mei X, Zhang T, Ouyang H, Lu B, Wang Z, Ji L. Scutellarin alleviates blood-retina-barrier oxidative stress injury initiated by activated microglia cells during the development of diabetic retinopathy. *Biochem Pharmacol.* 2019;159:82–95.
- Armulik A, Abramsson A, Betsholtz C. Endothelial/pericyte interactions. *Circ Res.* 2005;97:512–23.
- Morini MF, Giampietro C, Corada M, Pisati F, Lavarone E, Cunha SI, et al. VE-cadherin-mediated epigenetic regulation of endothelial gene expression. *Circ Res.* 2018;122:231–45.
- Cao R, Zhang Y. The functions of E(Z)/EZH2-mediated methylation of lysine 27 in histone H3. *Curr Opin Genet Dev.* 2004;14:155–64.
- Tang SL, Gao YL, Hu WZ. Scutellarin inhibits the metastasis and cisplatin resistance in glioma cells. *Onco Targets Ther.* 2019;12:587–98.
- Ke Y, Bao T, Wu X, Tang H, Wang Y, Ge J, et al. Scutellarin suppresses migration and invasion of human hepatocellular carcinoma by inhibiting the STAT3/Girdin/Akt activity. *Biochem Biophys Res Commun.* 2017;483:509–15.
- Li H, Huang D, Gao Z, Chen Y, Zhang L, Zheng J. Scutellarin inhibits the growth and invasion of human tongue squamous carcinoma through the inhibition of matrix metalloproteinase-2 and -9 and α v β 6 integrin. *Int J Oncol.* 2013;42:1674–81.
- Li CY, Wang Q, Wang X, Li G, Shen S, Wei X. Scutellarin inhibits the invasive potential of malignant melanoma cells through the suppression epithelial-mesenchymal transition and angiogenesis via the PI3K/Akt/mTOR signaling pathway. *Eur J Pharmacol.* 2019;858:172463.
- Hou L, Chen L, Fang L. Scutellarin inhibits proliferation, invasion, and tumorigenicity in human breast cancer cells by regulating HIPPO-YAP signaling pathway. *Med Sci Monit.* 2017;23:5130–8.
- Liu Y, Cao X. Characteristics and significance of the pre-metastatic niche. *Cancer Cell.* 2016;30:668–81.
- Corada M, Mariotti M, Thurston G, Smith K, Kunkel R, Brockhaus M, et al. Vascular endothelial-cadherin is an important determinant of microvascular integrity in vivo. *Proc Natl Acad Sci USA.* 1999;96:9815–20.
- Feldman GJ, Mullin JM, Ryan MP. Occludin: structure, function and regulation. *Adv Drug Deliv Rev.* 2005;57:883–917.
- Komarova YA, Kruse K, Mehta D, Malik AB. Protein interactions at endothelial junctions and signaling mechanisms regulating endothelial permeability. *Circ Res.* 2017;120:179–206.
- Conway DE, Breckenridge MT, Hinde E, Gratton E, Chen CS, Schwartz MA. Fluid shear stress on endothelial cells modulates mechanical tension across VE-cadherin and PECAM-1. *Curr Biol.* 2013;23:1024–30.
- Lertkiatmongkol P, Liao D, Mei H, Hu Y, Newman PJ. Endothelial functions of platelet/endothelial cell adhesion molecule-1 (CD31). *Curr Opin Hematol.* 2016;23:253–9.
- Chang CJ, Yang JY, Xia W, Chen CT, Xie X, Chao CH, et al. EZH2 promotes expansion of breast tumor initiating cells through activation of RAF1-beta-catenin signaling. *Cancer Cell.* 2011;19:86–100.
- Kleer CG, Cao Q, Varambally S, Shen R, Ota I, Tomlins SA, et al. EZH2 is a marker of aggressive breast cancer and promotes neoplastic transformation of breast epithelial cells. *Proc Natl Acad Sci USA.* 2003;100:11606–11.
- Kim KH, Roberts CW. Targeting EZH2 in cancer. *Nat Med.* 2016;22:128–34.
- Ning S, Ma X. Dephosphorylation-induced EZH2 activation mediated RECK downregulation by ERK1/2 signaling. *J Cell Physiol.* 2019;234:19010–8.
- Wan L, Xu K, Wei Y, Zhang J, Han T, Fry C, et al. Phosphorylation of EZH2 by AMPK suppresses PRC2 methyltransferase activity and oncogenic function. *Mol Cell.* 2018;69:279–91.
- Pan Z, Zhao W, Zhang X, Wang B, Wang J, Sun X, et al. Scutellarin alleviates interstitial fibrosis and cardiac dysfunction of infarct rats by inhibiting TGF β 1 expression and activation of p38-MAPK and ERK1/2. *Br J Pharmacol.* 2011;162:688–700.
- Martínez-Reza I, Díaz L, García-Becerra R. Preclinical and clinical aspects of TNF- α and its receptors TNFR1 and TNFR2 in breast cancer. *J Biomed Sci.* 2017;24:90.
- Vanamee ES, Faustman DL. TNFR2: a novel target for cancer immunotherapy. *Trends Mol Med.* 2017;23:1037–46.